Trapped Ion Mobility Spectrometry, Ultraviolet Photodissociation and ToF Mass Spectrometry for Gas-Phase Peptide Isobars/Isomers/Conformers Discrimination

Samuel A. Miller,[†,#] Kevin Jeanne Dit Fouque,[†,‡,#] Mark E. Ridgeway,[§] Melvin A. Park,[§] and Francisco Fernandez-Lima.*[,†,‡]

[†] Department of Chemistry and Biochemistry, Florida International University, Miami, FL 33199, United States.

[‡] Biomolecular Sciences Institute, Florida International University, Miami, FL 33199, United States.

[§] Bruker Daltonics Inc., Billerica, MA 01821, United States.

[#] These authors contributed equally to this work.

[*] Corresponding Author: Francisco Fernandez-Lima, Email: fernandf@fiu.edu.

ABSTRACT: Trapped ion mobility spectrometry (TIMS) when coupled with mass spectrometry (MS) offers great advantages for the separation of isobaric, isomeric and/or conformeric species. In the present work, we report the advantages of coupling TIMS with a low-cost UVPD enable linear ion trap operated at few 1-2 mbar prior to ToF MS analysis for the effective characterization of isobaric, isomeric and/or conformeric species based on mobility-selected fragmentation patterns. These three traditional challenges to MS-based separations are illustrated for the case of biologically relevant model systems: H3.1 histone tail PTM isobars (K4Me3/K18Ac), lanthipeptide regioisomers (overlapping/non-overlapping ring patterns), and a model peptide conformer (angiotensin I). The sequential nature of the TIMS operation allows for effective synchronization with the ToF MS scans, in addition to parallel operation between the TIMS and the UVPD trap. Inspection of the mobility selected UVPD MS spectra showed that for all three cases considered, unique fragmentation patterns (fingerprints) were observed per mobility band. Different from other IMS -UVPD implementations, the higher resolution of the TIMS device allowed for high mobility resolving power (R > 100) and effective mobility separation. The mobility selected UVPD MS provided high sequence coverage (>85%) with a fragmentation efficiency up to ~40%.

INTRODUCTION

The study of peptides and proteins in biological systems using mass spectrometry (MS)-based techniques has fundamentally advanced the understanding of the peptidomic/proteomic area over the years.[3-5] Significant advances in tandem mass spectrometry (MS/MS) have emerged based on complementary ion-activation methods for a more comprehensive structural characterization.[6-9] MS/MS-based techniques generate fragmentation patterns that lead to diagnostic fragment fingerprints, allowing for peptide/protein identification among other biomolecules. The most widely spread ion activation technique is low energy collision induced dissociation (CID), for which the ion internal energy is built-up by energetic collisions with neutral collision gas particles (e.g., N_2, Ar).[10, 11] This approach typically results in the cleavages of the peptide bond (N-C) for peptides/proteins, forming b_i/y_j series ions.[10, 12] However, low energy dissociation processes also lead to limited sequence coverage together with the absence of disulfide/thioether bond cleavages and the loss of labile post-translational modifications (PTMs).[13, 14]

To overcome the limited structural information from collision-based fragmentation techniques, alternative ion activation mechanisms, including electron-based (electron capture/transfer dissociation, ExD)[15] and photon-based (infrared multiphoton dissociation (IRMPD),[16] ultraviolet photodissociation (UVPD)[17]) fragmentation methods, have been developed to access new and complementary fragmentation pathways. ExD reactions primarily cleave the strongest N–Cα peptide backbone, while conserving the weakest C-N peptide bonds, generating c_i/z_j series ions from the dissociation of the charge-reduced $[M + zH]^{(z-1)\bullet}$ species.[15] These fragmentation techniques have significantly improved the characterization of peptides and proteins by providing complementary structural information to CID and increasing the sequence coverage.[8, 10, 14, 18, 19] In addition, ExD techniques afford several advantages over traditional collision-based methods in preserving the labile PTMs,[20, 21] conserving non-covalent interactions for the

identification of protein-ligand binding sites,[22, 23] and cleaving disulfide/thioether bonds.[2, 24] However, limitations to ExD are related to the dependence of the selected charge state precursor, low fragmentation efficiency and absence of fragmentation at proline residues.[15]

UVPD methods have gained significant attention in characterizing peptides and proteins.[7, 17, 25] UVPD relies on the absorption of UV photons that results in the electronic excitation of ions, for which direct dissociation from the exited states can be obtained through high energy dissociation pathways (a_i/x_j series ions unique to UVPD) and/or undergo relaxation processes involving lower energy fragmentation pathways (b_i, c_i /y_j, z_i series ions).[10, 17, 26-28] The ability of UVPD to produce a great diversity of product ions with higher fragmentation efficiency as compared to ECD, extensively increase the sequence coverage, improving the level of confidence for peptide and protein characterization. In addition, UVPD can preserve and localize PTMs[29, 30] and ligands binding sites[31, 32] as well as cleave disulfide/thioether bonds.[33, 34] All these features make the UVPD activation technique an interesting choice for proteomic applications.[35-37]

Several fragmentation methods have been previously developed with ion mobility spectrometry – mass spectrometry (IMS-MS) workflows (e.g., CID,[38-40] surface-induced dissociation (SID),[41, 42] ExD[43-45] and UVPD[46-49]). The integration of MS/MS events after the ion mobility separation allowed for the effective characterization of isomeric biomolecules based on their ion mobility-selected MS/MS spectra.[1, 47, 50-52] With the introduction of the electromagnetostatic (EMS) cell,[53] several groups have reported the benefit of ion mobility-selected ECD into commercially available IMS-q-ToF MS platforms (e.g., Agilent DTIMS-q-ToF MS,[54] Waters TWIMS-q-ToF MS[43] and Bruker TIMS-q-ToF MS[1, 55]). Custom built tandem drift tube IMS-MS (DTIMS-UVPD-DTIMS-q-ToF MS) have shown the potential of mobility-selected UVPD together with the ion mobility of the product ions for the characterization of biomolecules.[56] In addition, UVPD has also been integrated into IMS-MS commercial platforms prior to the IMS separation (e.g., a Waters Synapt G2 as q-UVPD-TWIMS-ToF MS[46] and a Bruker timsToF as TIMS-UVPD-TIMS-q-ToF MS[57]), for which product ions generated from UVPD events are separated in the ion mobility domain. Nevertheless, there is a need for the incorporation of low-cost high-resolution mobility analyzer (R > 100) prior to UVPD for the effective characterization of biomolecules of interest.

Here, we report, for the first time on the integration of TIMS and UVPD capabilities combined with ToF MS for the characterization of three common analytical challenges that require separation complementary to MS: i) lanthipeptide regioisomers (overlapping/non-overlapping ring patters), for which the formation of a specific ring pattern is typically critical to ensure the lanthipeptide bioactivity,[58-60] ii) H3.1 histone tail PTM isobars (K4Me3/K18Ac), for which combinatorial PTMs result in a histone code that are of particular interest due to their essential role in gene expression[61-63] and iii) gas-phase conformational isomers (angiotensin I) as a way to better understand the intramolecular interactions that stabilize gas-phase ions. The present TIMS combined with UVPD capabilities provides superior ion mobility separation when compared to previous IMS-UVPD implementations.[47, 56, 64] In the following discussion, a special emphasis is placed on the potential to acquire mobility related structural information using a low-cost UVPD enable linear ion trap, operated at high pressures (1-2 mbar) in tandem with the TIMS analyzer.

EXPERIMENTAL SECTION

Materials and Reagents. Lanthipeptide prochlorosins 3.3 (ProcA3.3 WT and ProcA3.3 C971H, GDTGIQAVLHTAGCYGGTKMCRA, 2255 Da) were expressed and purified as described elsewhere.[50] Histone H3.1 K4Me3, K9Me3, K23Me3, K27Me3, K18Ac, K27Ac and K36Ac tail peptides (ART**K**QTAR**K**STGGKAPR**K**QLATK-AAR**K**SAPATGGV**K**KPHRYRPGTVALRE, 5380 Da) were obtained from GenScript (Piscataway, NJ). Angiotensin I (DRVYIHPFHL, 1296 Da) was purchased from Sigma-Aldrich (Saint. Louis, MO). All peptide solutions were analyzed at a concentration of 10 µM prepared in 50:50 water/methanol (H_2O/MeOH) with 0.1% formic acid. A low concentration Tuning Mix standard (G1969-85000) was obtained from Agilent Technologies (Santa Clara, CA) and used for external ion mobility and mass calibration purposes.

TIMS-UVPD-ToF MS Instrumentation. The TIMS and UVPD capabilities were integrated on a Bruker Maxis Impact II ToF MS platform (Bruker Daltonics Inc., Billerica, MA), equipped with a nESI source operated in the positive ion mode. Figure 1a shows a simplified schematics of the nESI-TIMS-Trap UVPD section. A top view schematic is shown in the supplemental information (SchemeS1). A 213 nm laser beam, generated from the 5th harmonic of a Nd:YAG laser (NL204, EKSPLA, Vilnius, Lithuania), was operated at a repetition rate of 1 kHz with an energy of ~0.2 mJ per pulse with a 8 ns pulse width. The optical path consisted of UV mirrors used to guide the beam, UV CaF_2 flange-mounted windows (vacuum - atmosphere interface) and an optical shutter (SH-20, Electro-Optical Products Corp., Ridgewood, NY). The TIMS unit and the UVPD trap were controlled by a modular intelligent power source (MIPS, GAA Custom Electronics, WA), consisting of 16 channels with a 250 V output range and two rf drivers, and synchronized with the ToF-MS platform controls. The 203 mm long UVPD trap has a quadrupolar design (d0= 4.5 mm constructed of 4.0 mm round rods) and utilizes an

entrance (gate 1) and end (gate 2) lens system (~3 mm i.d. apertures).

The general fundamentals of TIMS and calibration procedures have been previously reported in the literature.[65-67] Briefly, the trapping of the ions in a TIMS device relies on the ability to generate a radially confining pseudopotential, through the action of an radiofrequency (rf) electrical potential applied to the electrodes of the TIMS analyzer, together with the generation of an axial electric field across the electrodes to counteract the drag force exerted by the gas flow. The nESI emitters were pulled in-house from quartz capillaries (O.D. = 1.0 mm and I.D. = 0.70

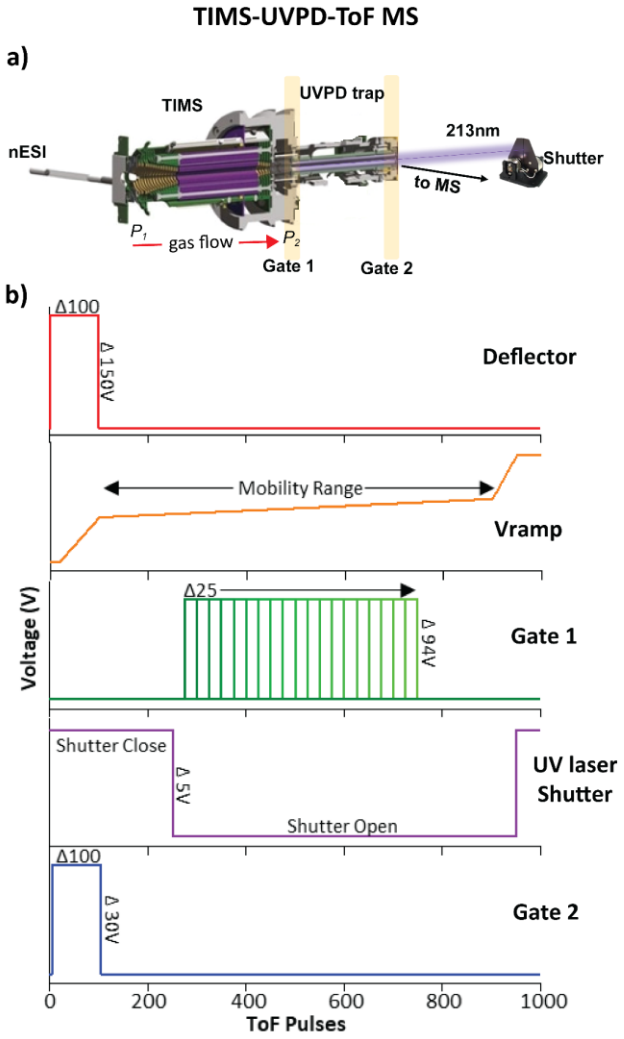

Figure 1. (a) Schematic of the nESI-TIMS-UVPD segment of the nESI-TIMS-UVPD-ToF MS instrument, (b) Timing sequences occurring during TIMS-UVPD experiments. Note that the ΔV refers to the difference between the open and close voltages for each of the TIMS-UVPD component, while the ΔToF pulses refer to the time the window of voltages stays open during TIMS-UVPD acquisition.

mm) using a Sutter Instrument Co. P2000 laser puller. Peptide sample solutions were loaded in a pulled-tip capillary, housed in a mounted custom built XYZ stage in front of the MS inlet, and sprayed at ~900-1100 V via a tungsten wire inserted inside the nESI emitters. TIMS experiments were performed using nitrogen (N_2) at ambient temperature (T) with a gas velocity (v_g) defined by the funnel entrance (P_1 = 4.5 mbar) and exit (P_2 = 1.8 mbar) pressure differences (Figure 1a). TIMS was operated using an rf voltage of 320 Vpp at 720 kHz and the UVPD trap using an rf voltage of 170 Vpp at 675 kHz. A deflector voltage of 300 V, a TIMS exit lens (gate 1) of 169 V, a multipole exit lens (gate 2) of 135 V as well as a ramp voltage of -70 to 0 V (lanthipeptides), -40 to 5 V (histone tails) and -50 to -20 V (angiotensin I) were used for the ion mobility separations. The scan rate ($Sr = \Delta V_{ramp}/t_{ramp}$) was optimized for high mobility separation. All resolving power (R) and resolution (r) values reported herein were determined as $R = \Omega/w$ and $r = 1.18*(\Omega_2-\Omega_1)/(w_1+w_2)$, where Ω and w are collision cross sections (CCS) and the full peak width at half maximum (FWHM) of the IMS profile.

During parallel TIMS and UVPD operation, ion mobility selected ions are UV irradiated with ~ 225 laser pulses (225 ms trap time) in the UVPD trap while the ion mobility TIMS experiment occurs. The ion mobility experiment (225 ms) consists of 1000 ToF MS events. The timing sequence and ToF pulse profiles for the TIMS operation are described in Figure 1b. Briefly, ions are orthogonally deflected into the TIMS device (open for 100 ToF MS pulses using a Δ150 V at the deflector), trapped and eluted using a non-linear ramp scan such that high ion mobility resolution (R > 100) is achieved over the ion mobility range of interest.[68] In the described experiments, the analytical section of the nonlinear ramp consisted of a ΔV_{ramp} of 70 V (lanthipeptides), 45 V (histone tails), and 30 V (angiotensin I). The ion mobility range of interest (250-800 ToF pulse range) that is transfer into the UVPD trap is defined by the gate 1 (pulse delay, width, step and operating voltages); typical gate 1 pulse width, step and operating voltages are 25 pulse pulses, 25 pulse pulses and $\Delta V_{Gate\ 1}$ of 94 V. The UVPD events are synchronized with the TIMS experiments using the gate 1 and gate 2, and a shutter that opens for 700 ToF pulses using a ΔV of 5 V). After fragmentation, the ions are eluted from the UVPD trap using the multipole exit lens system (gate 2 opens for 100 ToF pulses using a ΔV of 30 V), and deflected orthogonally towards the electrodynamic entrance funnel of the ToF MS.

Each experiment typically lasted 3-5 min, depending on the number of mobility windows of interest. A smaller inner diameter lens located between the TIMS and the trap region allows for maximum UVPD fragmentation in the trap region and minimal UV light transmission to the TIMS region. Potential UVPD product ions from the TIMS analyzer (<50% efficiency) are excluded by their ion

mobility to enter the trap region. Data was processed using Data Analysis 5.1 (Bruker Daltonics). The UVPD fragmentation efficiency was defined by the ratio of the precursor ions between the similar time length shutter open and close events. The MS fragment ion annotations were performed using a custom excel table with all theoretical combinations of fragments based on the peptide sequence. The fragment ions were assigned with a mass error of ~15 ppm average with S/N of ~6-7 in the UVPD spectra.

RESULTS AND DISCUSSION

TIMS-UVPD-ToF MS experiments were conducted on three systems of interest: $[M + 3H]^{3+}$ ions of isomeric lanthipeptides, $[M + 10H]^{10+}$ ions of histone tails with varying PTM position, and $[M + 2H]^{2+}$ ions of conformeric species in angiotensin I. Note that the precursor ions were selected in the mobility domain without m/z selection in the UVPD spectra. A comparison between IMS/MS spectra per ion mobility band when the 213 nm UV laser shutter is close (top) and open (bottom) can be found in Figure S1 for all investigated binary mixtures.

TIMS-UVPD-ToF MS of Isomeric ProcA3.3 Lanthipeptides. The performance evaluation of the TIMS-UVPD-ToF MS workflow was first investigated using lanthipeptides, which are a structurally unique class of ribosomally synthesized and post-translationally modified peptides (RiPPs).[69] They are characterized by intramolecular β-thioether cross-links formed between a dehydrated serine/threonine (dSer/dThr) and a cysteine residue (Figure 2) through the action of lanthipeptide synthetases. These lanthipeptides are also known to exert various biological activities.[69] In vitro/vivo studies showed that the lanthipeptide synthetase ProcM could alter and produce highly diverse lanthipeptide ring patterns (overlapping and non-overlapping rings).[70, 71] The formation of a specific ring pattern is typically critical to ensure the lanthipeptide bioactivity.[58, 60]

Two isomeric prochlorosins, ProcA3.3 WT (overlapping ring) and ProcA3.3 C971H (non-overlapping ring), with previously reported lanthipeptide ring patterns,[72] were investigated in a binary mixture. Typical ion mobility, precursor ion mass with UV laser shutter open/close and ion mobility selected UVPD spectra of the ProcA3.3 WT (blue) and ProcA3.3 C971H (red) $[M + 3H]^{3+}$ molecular species are illustrated in Figure 2. The two isomeric species were baseline separated in TIMS, with an apparent ion mobility $R \sim 110$ and $r \sim 3.6$ using a $Sr = 0.31$ V/ms, where the overlapping ring pattern from ProcA3.3 WT exhibited more compact structures (~585 Å^2) as compared to the non-overlapping ring pattern from ProcA3.3 C971H (640 Å^2) consistent with previous TIMS-MS reports (Figure 2a).[50] Differences in the isotopic pattern distribution

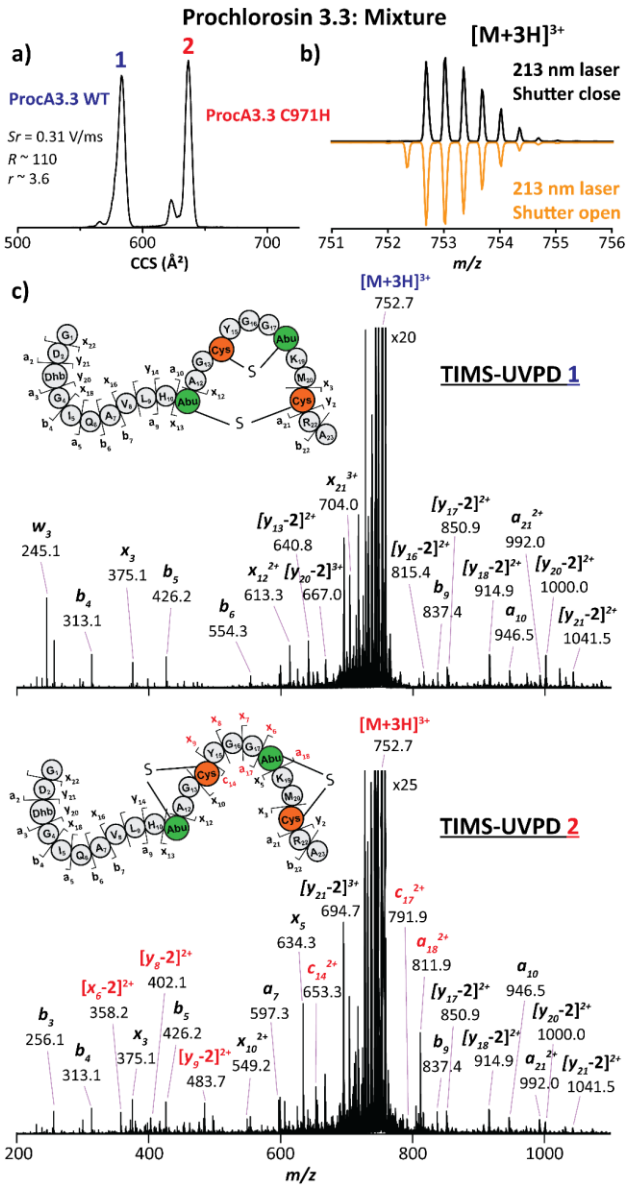

Figure 2. TIMS-UVPD-ToF MS analysis of the selected $[M + 3H]^{3+}$ species of ProcA3.3 WT (blue) and ProcA3.3 C971H (red) isomeric lanthipeptides (m/z 752.7). (a) TIMS profile in a binary mixture, (b) isotopic pattern distribution of the precursor ion produced with UV laser shutter close (top) and shutter on (bottom). (c) Ion mobility UVPD-IMS/MS spectra. Typical non-overlapping ring pattern specific product ions are highlighted in red. The residues involved in the thioether cross-link are colored in orange (former Cys) and green (former Thr), respectively.

were observed for the precursor ions (m/z 539) upon UVPD, where a loss of 1 or 2 hydrogen atoms were obtained (Figure 2b). Consequently, these ions appear to be signature ions of the UVPD events and corroborate that hydrogen-transfer processes are involved during the

absorption/dissociation events in agreement with prior UVPD studies.[73, 74]

Common a_i, b_i/x_j, y_j product ions were observed outside of the thioether ring region (dThr11-Cys21 residues) for the two isomeric species (Figure 2c). However, specific fragments were observed in the Tyr15-Gly17 residue region for the IMS band 2, confirming the presence of a non-overlapping lanthipeptide ring pattern,[2, 50, 70] while the UVPD data were consistent with an overlapping lanthipeptide ring pattern (no fragmentation in the Tyr15-Gly17 region) for the IMS band 1 (Figure 2c). In addition, UVPD fragmentation may involve radical-driven processes that can induce dissociation in the disulfide/thioether bonds as previously described.[33, 34] Differences in the UVPD fragmentation pattern were observed near the thioether rings. Here cleavages at each extremity of the residues involved in the two thioether rings (dThr11/Cys14 and dThr18/Cys21 residues) were observed for the non-overlapping ring pattern, while only cleavages at each extremity of the residues involved in the largest thioether ring (dThr11/Cys21 residues) were obtained for the overlapping ring pattern (Figure 2c). This suggests that the UVPD radical-driven processes cannot cleave multiple thioether bonds at the same time. Indeed, cleavages may occur in the smallest thioether bond (Cys14/dThr18 residues) of the overlapping ring, but fragments will remain attached to the backbone by the second thioether bond (dThr11/Cys21 residues). Consequently, UVPD can also assign the residues involved in the thioether cross-links.

The ion mobility selected UVPD spectra permitted a clear ion mobility separation together with lanthipeptide ring pattern assignment with a sequence coverage of ~65% (overlapping) and 87% (non-overlapping) with UVPD fragmentation efficiency of ~10% (Figure S2) for the two ProcA3.3 WT and ProcA3.3 C971H lanthipeptide isomers. The present TIMS-UVPD-ToF MS workflow proved to be a more efficient approach than traditional TIMS-q-CID-ToF MS/MS and TIMS-q-ECD-ToF MS/MS techniques[2, 50] for the characterization of lanthipeptide ring patterns by providing higher fragmentation efficiency between the two non-overlapping rings as well as unique cleavages at residues involved in the thioether rings, making less ambiguous the assignment of the lanthipeptide ring connectivity. All these features make UVPD a very well-suited alternative to CID and ECD for the discrimination of lanthipeptide ring patterns.

TIMS-UVPD-ToF MS of Isobaric histone H3.1 PTM Tails. The potential of the TIMS-UVPD-ToF MS platform was also evaluated using a binary mixture of isobaric K4Me3 and K18Ac histone tail proteoforms.

Histones consist of ~100-150 residues, for which most of the PTMs (at diverse and/or multiple sites) are located in the N-terminal part of the proteins, so-called histone tails, that protrude from the nucleosome.[62, 75, 76] Combinatorial PTMs result in a histone code that are of particular interest due to their essential role in gene expression.[62, 63] However, the enzymatic machinery that establishes the histone code can be deregulated in cancer leading to alterations in the PTM patterns having crucial functions in diverse cancer development and progression.[77, 78]

Typical ion mobility, precursor ion mass with UV laser shutter open/close and ion mobility selected UVPD spectra of the K4Me3 (green) and K18Ac (blue) $[M + 10H]^{10+}$ molecular species are illustrated in Figure 3. The charge state 10+ was selected based on previous TIMS-MS studies, for which the two isobaric species exhibited differences in CCS (~ 40 Å^2) as well as relatively simple ion mobility distributions (mainly one IMS band).[1, 79] The TIMS analysis resulted in the separation of the two isobaric species, with an apparent ion mobility $R \sim 140$ and $r \sim 1.3$ using a $Sr = 0.20$ V/ms, where K18Ac exhibited more compact structures (~1805 Å^2) as compared to K4Me3 (1845 Å^2) consistent with previous TIMS-MS reports (Figure 3a).[1, 79] The presence of a loss of 1 or 2 hydrogen atoms in the isotopic pattern distribution of the precursor ions (m/z 539) was observed when the shutter of the UV laser was open as signature ions of UVPD events.

Common a_i, b_i, c_i/x_j, y_j, z_j product ions were observed for the two isobaric species in the Lys18-Arg49 residue region, corresponding to either fragments comprising the PTM (toward the N-terminal) or fragments not containing the PTM (toward the C-terminal, Figure 3c). However, a shift of 42 Da was only observed in the Lys4-Arg17 residue region for the IMS band 2, confirming the PTM localization at position 4 while the UVPD data were consistent with PTM localization at position 18 for the IMS band 1 (Figure 3c). The ion mobility selected UVPD spectra permitted a clear ion mobility separation together with PTM localization with a sequence coverage of ~82% and UVPD fragmentation efficiency of ~40% (Figure S2) for the two K4Me3 and K18Ac histone tail proteoforms. The present TIMS-UVPD spectra displayed similar sequence coverage as compared to recently reported traditional TIMS-ECD data (~86%) but presented much higher fragmentation efficiency as compared to ECD (~10%).[1] Other histone tails with varying PTM position also showed similar sequence coverage and fragmentation efficiency (Figures S3-S7). These features make UVPD a very well-suited alternative to ECD for the discrimination of histone tail proteoforms. Potential challenges associated with the IMS isolation of the precursor ions of interest are interferences from endogenous molecules and other charge states with similar ion mobilities, as reflected in Figure S8 for the case of histone tails. To account for that, future implementation can consider the use of complementary chromatographic and/or MS separations prior to the IMS domain. This is beyond the focus of the present study, where we are more focusing on the UVPD implementation at higher pressures in low-cost, linear ion trap set-up operating at 1-2 mbar.

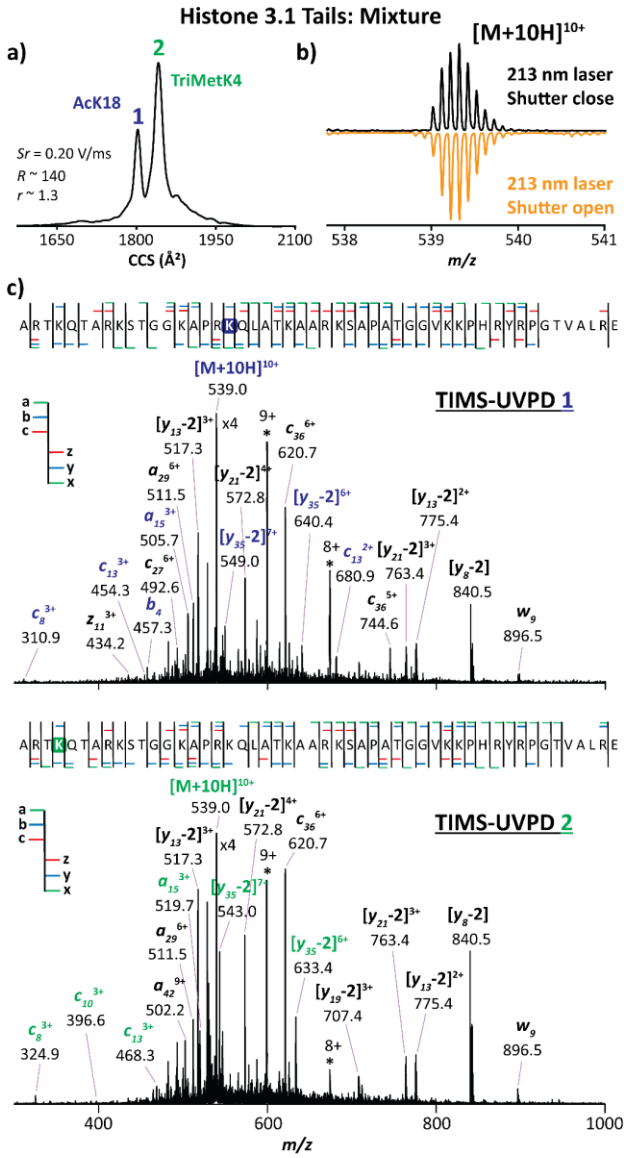

Figure 3. TIMS-UVPD-ToF MS analysis of the selected [M + 10]$^{10+}$ species of K18Ac (blue) and K4Me3 (green) isobaric histone tails (*m/z* 539.0). (a) TIMS profile in a binary mixture, (b) isotopic pattern distribution of the precursor ion produced with UV laser shutter close (top) and with shutter open (bottom). (c) Ion mobility UVPD-IMS/MS spectra. The fragments comprising the PTM are highlighted in blue and green for K18Ac and K4Me3, respectively.

TIMS-UVPD-ToF MS of Conformational Isomeric Angiotensin I. The novel implementation of the TIMS-UVPD-ToF MS platform was also evaluated using the model peptide angiotensin I for direct comparison with recently reported TIMS-q-ECD MS/MS data, where ion mobility-selected ECD spectra provided fingerprints associated with the gas-phase conformational isomers.[55] The TIMS-q-ECD MS/MS results suggested that the two most compact structures (IMS 1/2 bands) involve an His6-Pro7 peptide bond in a *trans*-configuration, while the most extended structure (IMS 3 band) have the Pro7 in a *cis*-configuration.

Typical ion mobility, precursor ion mass with UV laser shutter open/close and relative intensity of observed UVPD fragments per IMS band of the angiotensin I [M + 2H]$^{2+}$ molecular species are shown in Figure 4.

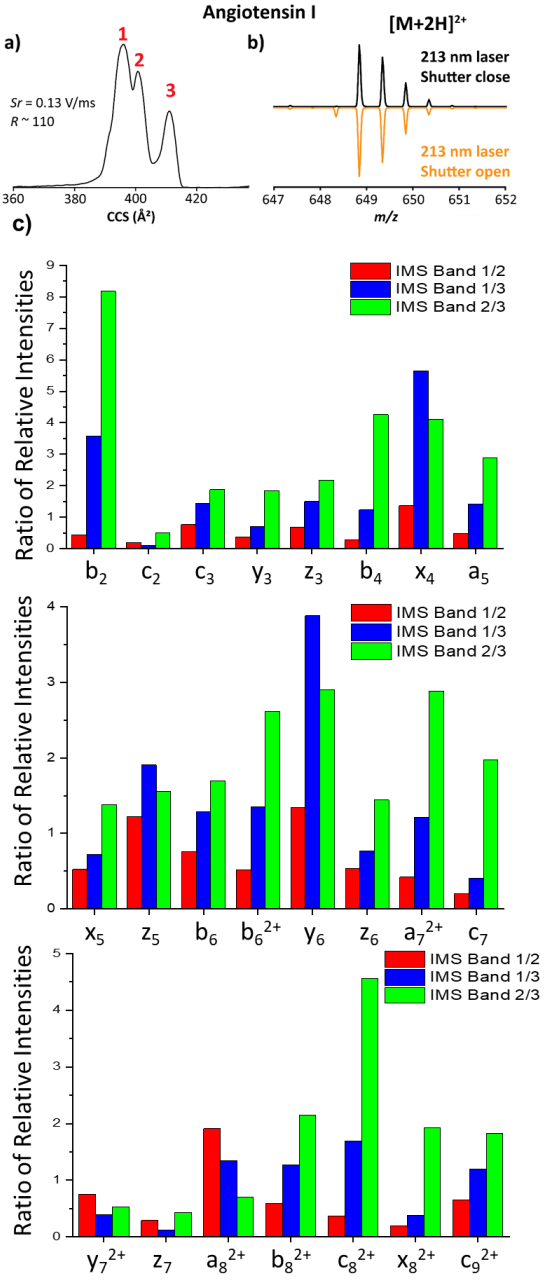

Figure 4. TIMS-UVPD-ToF MS analysis of the selected [M + 2H]$^{2+}$ species of angiotensin I (*m/z* 648.9). (a) TIMS profile, (b) isotopic pattern distribution of the precursor ion produced with UV laser shutter close (top) and with shutter open (bottom) and (c) ratio of the relative intensities per IMS band 1-3 (data shown for variations larger than ±0.20, see

supporting information Figure S9 and Table S1 for more details)

The TIMS analysis from the TIMS-UVPD-ToF MS platform was consistent with the one obtained using the TIMS-q-ECD-ToF MS/MS platform,[55] for which three IMS bands were obtained (396 Å^2, 401 Å^2 and 411 Å^2), with an apparent ion mobility $R \sim 110$ using a Sr = 0.13 V/ms (Figure 4a). The altered isotopic pattern distribution of the precursor ions (m/z 648), when laser was activated, attested for UVPD events (Figure 4b). No major changes in the mobility-selected fragmentation spectra was observed across replicas.

Inspection of the ion mobility selected UVPD spectra exhibited similar fragmentation patterns across the IMS bands, for which common a_i, b_i, c_i/x_j, y_j, z_j product ions were observed through the angiotensin I sequence (Figure 4c and S9). Moreover, based on the changes of the ratio of the relative intensities of the fragments a memory effect of the gas-phase conformation was observed (Figure 4c).

Overall, the relative abundance of fragments located in the Asp1-Tyr4 residue region was low and similar across the IMS bands, consistent with the notion that the bulky side chain of Tyr4 together with the basic Arg2 residue that lock this part of the structure in a way that limit high abundance residue cleavages. However, differences in the relative abundance were observed in the Ile5-Leu10 region across the ion mobility selected UVPD spectra. One of the major differences was located at the His6-Pro7 peptide bond, where the b_6 product ions exhibited lower abundances for the IMS 3 band as compared to IMS 1/2 bands. This is consistent with the idea that the Pro7 residue adopts a *cis*-configuration for the IMS 3 band, while probably having a *trans*-configuration for the IMS 1/2 bands, in good agreement with recently reported ion mobility selected ECD results.[55] Another significant difference was found at the c_9 product ions (Figure 4c), where a lower relative abundance was observed for IMS 3 band, while increasing toward the IMS band 1. This is consistent with the idea that the His9-Leu10 peptide bond becomes more accessible for cleavage once the Pro7 adopts a *trans*-configuration, while the *cis*-configuration makes the cleavage between His9 and Leu10 residues less accessible. This feature can be explained by the close proximity of the bulky side chain of Phe8, while being further away when Pro7 is in a *cis*-configuration and then could be in closer proximity to the Asp1-Tyr4 region in agreement with more compact structures.

The ion mobility selected UVPD spectra permitted angiotensin I ion mobility separated conformer assignment, in agreement with previous ion mobility selected ECD spectra,[55] with a complete sequence coverage and UVPD fragmentation efficiency of ~12% (Figure S2). In addition, the present TIMS-UVPD-ToF MS workflow exhibited higher fragmentation efficiency as compared to the TIMS-q-ECD-ToF MS/MS platform (5%),[55] making less ambiguous the tentative assignment of angiotensin I conformers. The presented results showcased the potential of UVPD as a very well-suited alternative to traditional CID and ExD workflow for the discrimination of conformers.

CONCLUSION

The advantages of coupling TIMS with a UVPD enable linear ion trap operated at few 1-2 mbar prior to ToF MS analysis for the effective characterization of isobaric, isomeric and/or conformeric species based on mobility-selected fragmentation patterns is described. The TIMS operation using a linear scan function and mobility gating allows for selected ion mobility packages to be transferred into the UVPD trap for photodissociation followed by ToF MS detection. The sequential nature of the TIMS operation allows for effective synchronization with the ToF MS scans, in addition to parallel operation between the TIMS and the UVPD trap. As a result, ion mobility selected UVPD-ToF MS spectra were collected by stepping the ion mobility window across the ion mobility range of interest. Different from other IMS implementations, the higher resolution of the TIMS device allows for high mobility resolving power (R > 100) now in tandem with UVPD fragmentation.

The application of the present workflow is successfully illustrated for the characterization of model peptide conformers (angiotensin I), lanthipeptide regioisomers (overlapping/non-overlapping ring patters) and H3.1 histone tail PTM isobars (K4Me3/K18Ac). The UVPD fragmentation spectra showed characteristic (a_i/x_j series ions unique to UVPD) as well as lower energy fragmentation pathways (b_i, c_i /y_j, z_i series ions). In addition, conformer and sequence specific fragmentation patterns were observed with high coverage (>85%). When compared to other 'non-ergodic' fragmentation strategies (e.g., recently implemented TIMS-ECD-q-ToF MS),[1, 55] a significantly higher fragmentation efficiency (up to ~40%) was obtained for UVPD, facilitating the structural characterization of the ion mobility selected gas-phase molecular ions. This platform shows promise for the analysis of intact histones with varying PTMs, as well as further interpretation of the structural motifs that drive the gas-phase conformational states of biomolecular ions. Results showed that effective UVPD fragmentation can be achieved at 1-2 mbar; that is the fragmentation mechanism dominates over potential collisional dampening.

ASSOCIATED CONTENT

Supporting Information

The Supporting Information is available free of charge at http://pubs.acs.org. Simplified schematics of the nESI-TIMS-Trap UVPD section integrated into an existing Bruker Maxis

Impact II ToF MS platform. IMS/MS spectra of UV laser shutter close/open for all investigated binary mixtures and UVPD fragmentation efficiencies. TIMS-UVPD-ToF MS analysis of the [M + 10H]10+ species of K9Me3, K23Me3, K27Me3, K27Ac and K36Ac. 2D-TIMS-MS contour map and extracted IMS spectra for the 8+-10+ species of K23Me3. Bar plots and Table containing the fragments per IMS band of the TIMS-UVPD-ToF MS analysis of the angiotensin I 2+ (m/z 648.9).

AUTHOR INFORMATION

Corresponding Author

Francisco Fernandez-Lima, Email: fernandf@fiu.edu

Notes

MER and MAP are employed by Bruker Daltonics – a manufacturer of TIMS.

ACKNOWLEDGEMENTS

The authors at FIU acknowledge the financial support from the National Science Foundation Division of Chemistry, under CAREER award CHE-1654274, with co-funding from the Division of Molecular and Cellular Biosciences to FFL and funding from National Institutes of General Medicine (R01GM134247). We also thank Dr. Jennifer Brodbelt for helpful discussions during the design and implementation of the UVPD experiments.

REFERENCES

1. Jeanne Dit Fouque, K.; Kaplan, D.; Voinov, V. G.; Holck, F. H. V.; Jensen, O. N.; Fernandez-Lima, F., Proteoform Differentiation using Tandem Trapped Ion Mobility, Electron Capture Dissociation, and ToF Mass Spectrometry. *Anal. Chem.* **2021,** *93* (27), 9575-9582.
2. Jeanne Dit Fouque, K.; Hegemann, J. D.; Santos-Fernandez, M.; Le, T. T.; Gomez-Hernandez, M.; van der Donk, W. A.; Fernandez-Lima, F., Exploring structural signatures of the lanthipeptide prochlorosin 2.8 using tandem mass spectrometry and trapped ion mobility-mass spectrometry. *Anal. Bioanal. Chem.* **2021,** *413* (19), 4815-4824.
3. Aebersold, R.; Mann, M., Mass spectrometry-based proteomics. *Nature* **2003,** *422* (6928), 198-207.
4. Han, X.; Aslanian, A.; Yates, J. R., 3rd, Mass spectrometry for proteomics. *Curr. Opin. Chem. Biol.* **2008,** *12* (5), 483-490.
5. Yates, J. R.; Ruse, C. I.; Nakorchevsky, A., Proteomics by mass spectrometry: approaches, advances, and applications. *Annu. Rev. Biomed. Eng.* **2009,** *11*, 49-79.
6. Zhang, Y.; Fonslow, B. R.; Shan, B.; Baek, M. C.; Yates, J. R., 3rd, Protein analysis by shotgun/bottom-up proteomics. *Chem. Rev.* **2013,** *113* (4), 2343-2394.
7. Shaw, J. B.; Li, W.; Holden, D. D.; Zhang, Y.; Griep-Raming, J.; Fellers, R. T.; Early, B. P.; Thomas, P. M.; Kelleher, N. L.; Brodbelt, J. S., Complete protein characterization using top-down mass spectrometry and ultraviolet photodissociation. *J. Am. Chem. Soc.* **2013,** *135* (34), 12646-12651.
8. Mikesh, L. M.; Ueberheide, B.; Chi, A.; Coon, J. J.; Syka, J. E.; Shabanowitz, J.; Hunt, D. F., The utility of ETD mass spectrometry in proteomic analysis. *Biochim. Biophys. Acta* **2006,** *1764* (12), 1811-1822.
9. Shaw, J. B.; Malhan, N.; Vasil'ev, Y. V.; Lopez, N. I.; Makarov, A.; Beckman, J. S.; Voinov, V. G., Sequencing Grade Tandem Mass Spectrometry for Top-Down Proteomics Using Hybrid Electron Capture Dissociation Methods in a Benchtop Orbitrap Mass Spectrometer. *Anal. Chem.* **2018,** *90* (18), 10819-10827.
10. Brodbelt, J. S., Ion Activation Methods for Peptides and Proteins. *Anal. Chem.* **2016,** *88* (1), 30-51.
11. McLuckey, S. A., Principles of collisional activation in analytical mass spectrometry. *J. Am. Soc. Mass Spectrom.* **1992,** *3* (6), 599-614.
12. Mitchell Wells, J.; McLuckey, S. A., Collision-Induced Dissociation (CID) of Peptides and Proteins. *Methods Enzymol.* **2005,** *402*, 148-185.
13. Paizs, B.; Suhai, S., Fragmentation pathways of protonated peptides. *Mass Spectrom. Rev.* **2005,** *24* (4), 508-548.
14. Jeanne Dit Fouque, K.; Lavanant, H.; Zirah, S.; Hegemann, J. D.; Fage, C. D.; Marahiel, M. A.; Rebuffat, S.; Afonso, C., General rules of fragmentation evidencing lasso structures in CID and ETD. *Analyst* **2018,** *143* (5), 1157-1170.
15. Zhurov, K. O.; Fornelli, L.; Wodrich, M. D.; Laskay, U. A.; Tsybin, Y. O., Principles of electron capture and transfer dissociation mass spectrometry applied to peptide and protein structure analysis. *Chem. Soc. Rev.* **2013,** *42* (12), 5014-5030.
16. Brodbelt, J. S.; Wilson, J. J., Infrared multiphoton dissociation in quadrupole ion traps. *Mass Spectrom. Rev.* **2009,** *28* (3), 390-424.
17. Brodbelt, J. S.; Morrison, L. J.; Santos, I., Ultraviolet Photodissociation Mass Spectrometry for Analysis of Biological Molecules. *Chem. Rev.* **2020,** *120* (7), 3328-3380.
18. Kim, M. S.; Zhong, J.; Kandasamy, K.; Delanghe, B.; Pandey, A., Systematic evaluation of alternating CID and ETD fragmentation for phosphorylated peptides. *Proteomics* **2011,** *11* (12), 2568-2572.
19. Sobott, F.; Watt, S. J.; Smith, J.; Edelmann, M. J.; Kramer, H. B.; Kessler, B. M., Comparison of CID versus ETD based MS/MS fragmentation for the analysis of protein ubiquitination. *J. Am. Soc. Mass Spectrom.* **2009,** *20* (9), 1652-1659.
20. Jung, H. R.; Sidoli, S.; Haldbo, S.; Sprenger, R. R.; Schwammle, V.; Pasini, D.; Helin, K.; Jensen, O. N., Precision mapping of coexisting modifications in histone H3 tails from embryonic stem cells by ETD-MS/MS. *Anal. Chem.* **2013,** *85* (17), 8232-8239.
21. Han, L.; Costello, C. E., Electron transfer dissociation of milk oligosaccharides. *J. Am. Soc. Mass Spectrom.* **2011,** *22* (6), 997-1013.
22. Xie, Y.; Zhang, J.; Yin, S.; Loo, J. A., Top-down ESI-ECD-FT-ICR mass spectrometry localizes noncovalent protein-ligand binding sites. *J. Am. Chem. Soc.* **2006,** *128* (45), 14432-14433.
23. Jackson, S. N.; Dutta, S.; Woods, A. S., The use of ECD/ETD to identify the site of electrostatic interaction in noncovalent complexes. *J. Am. Soc. Mass Spectrom.* **2009,** *20* (2), 176-179.
24. Tan, L.; Durand, K. L.; Ma, X.; Xia, Y., Radical cascades in electron transfer dissociation (ETD) - implications for characterizing peptide disulfide regio-isomers. *Analyst* **2013,** *138* (22), 6759-6765.
25. Brodbelt, J. S., Photodissociation mass spectrometry: new tools for characterization of biological molecules. *Chem. Soc. Rev.* **2014,** *43* (8), 2757-2783.

26. Antoine, R.; Dugourd, P., Visible and ultraviolet spectroscopy of gas phase protein ions. *Phys. Chem. Chem. Phys.* **2011,** *13* (37), 16494-16509.

27. Zabuga, A. V.; Kamrath, M. Z.; Boyarkin, O. V.; Rizzo, T. R., Fragmentation mechanism of UV-excited peptides in the gas phase. *J. Chem. Phys.* **2014,** *141* (15), 154309.

28. Julian, R. R., The Mechanism Behind Top-Down UVPD Experiments: Making Sense of Apparent Contradictions. *J. Am. Soc. Mass Spectrom.* **2017,** *28* (9), 1823-1826.

29. Cleland, T. P.; DeHart, C. J.; Fellers, R. T.; VanNispen, A. J.; Greer, J. B.; LeDuc, R. D.; Parker, W. R.; Thomas, P. M.; Kelleher, N. L.; Brodbelt, J. S., High-Throughput Analysis of Intact Human Proteins Using UVPD and HCD on an Orbitrap Mass Spectrometer. *J. Proteome Res.* **2017,** *16* (5), 2072-2079.

30. Greer, S. M.; Sidoli, S.; Coradin, M.; Schack Jespersen, M.; Schwammle, V.; Jensen, O. N.; Garcia, B. A.; Brodbelt, J. S., Extensive Characterization of Heavily Modified Histone Tails by 193 nm Ultraviolet Photodissociation Mass Spectrometry via a Middle-Down Strategy. *Anal. Chem.* **2018,** *90* (17), 10425-10433.

31. Sipe, S. N.; Patrick, J. W.; Laganowsky, A.; Brodbelt, J. S., Enhanced Characterization of Membrane Protein Complexes by Ultraviolet Photodissociation Mass Spectrometry. *Anal. Chem.* **2020,** *92* (1), 899-907.

32. Escobar, E. E.; King, D. T.; Serrano-Negron, J. E.; Alteen, M. G.; Vocadlo, D. J.; Brodbelt, J. S., Precision Mapping of O-Linked N-Acetylglucosamine Sites in Proteins Using Ultraviolet Photodissociation Mass Spectrometry. *J. Am. Chem. Soc.* **2020,** *142* (26), 11569-11577.

33. Bonner, J.; Talbert, L. E.; Akkawi, N.; Julian, R. R., Simplified identification of disulfide, trisulfide, and thioether pairs with 213 nm UVPD. *Analyst* **2018,** *143* (21), 5176-5184.

34. Agarwal, A.; Diedrich, J. K.; Julian, R. R., Direct elucidation of disulfide bond partners using ultraviolet photodissociation mass spectrometry. *Anal. Chem.* **2011,** *83* (17), 6455-6458.

35. Fort, K. L.; Dyachenko, A.; Potel, C. M.; Corradini, E.; Marino, F.; Barendregt, A.; Makarov, A. A.; Scheltema, R. A.; Heck, A. J., Implementation of Ultraviolet Photodissociation on a Benchtop Q Exactive Mass Spectrometer and Its Application to Phosphoproteomics. *Anal. Chem.* **2016,** *88* (4), 2303-10.

36. Greer, S. M.; Parker, W. R.; Brodbelt, J. S., Impact of Protease on Ultraviolet Photodissociation Mass Spectrometry for Bottom-up Proteomics. *J. Proteome Res.* **2015,** *14* (6), 2626-2632.

37. Fornelli, L.; Srzentic, K.; Toby, T. K.; Doubleday, P. F.; Huguet, R.; Mullen, C.; Melani, R. D.; Dos Santos Seckler, H.; DeHart, C. J.; Weisbrod, C. R.; Durbin, K. R.; Greer, J. B.; Early, B. P.; Fellers, R. T.; Zabrouskov, V.; Thomas, P. M.; Compton, P. D.; Kelleher, N. L., Thorough Performance Evaluation of 213 nm Ultraviolet Photodissociation for Top-down Proteomics. *Mol. Cell. Proteomics* **2020,** *19* (2), 405-420.

38. Lee, Y. J.; Hoaglund-Hyzer, C. S.; Taraszka, J. A.; Zientara, G. A.; Counterman, A. E.; Clemmer, D. E., Collision-induced dissociation of mobility-separated ions using an orifice-skimmer cone at the back of a drift tube. *Anal. Chem.* **2001,** *73* (15), 3549-3555.

39. Pringle, S. D.; Giles, K.; Wildgoose, J. L.; Williams, J. P.; Slade, S. E.; Thalassinos, K.; Bateman, R. H.; Bowers, M. T.; Scrivens, J. H., An investigation of the mobility separation of some peptide and protein ions using a new hybrid quadrupole/travelling wave IMS/oa-ToF instrument. *Int. J. Mass Spectrom.* **2007,** *261* (1), 1-12.

40. Becker, C.; Fernandez-Lima, F. A.; Gillig, K. J.; Russell, W. K.; Cologna, S. M.; Russell, D. H., A novel approach to collision-induced dissociation (CID) for ion mobility-mass spectrometry experiments. *J. Am. Soc. Mass Spectrom.* **2009,** *20* (6), 907-914.

41. Zhou, M.; Huang, C.; Wysocki, V. H., Surface-induced dissociation of ion mobility-separated noncovalent complexes in a quadrupole/time-of-flight mass spectrometer. *Anal. Chem.* **2012,** *84* (14), 6016-6023.

42. Panczyk, E. M.; Snyder, D. T.; Ridgeway, M. E.; Somogyi, A.; Park, M. A.; Wysocki, V. H., Surface-Induced Dissociation of Protein Complexes Selected by Trapped Ion Mobility Spectrometry. *Anal. Chem.* **2021,** *93* (13), 5513-5520.

43. Williams, J. P.; Morrison, L. J.; Brown, J. M.; Beckman, J. S.; Voinov, V. G.; Lermyte, F., Top-Down Characterization of Denatured Proteins and Native Protein Complexes Using Electron Capture Dissociation Implemented within a Modified Ion Mobility-Mass Spectrometer. *Anal. Chem.* **2020,** *92* (5), 3674-3681.

44. Kolli, V.; Schumacher, K. N.; Dodds, E. D., Ion mobility-resolved collision-induced dissociation and electron transfer dissociation of N-glycopeptides: gathering orthogonal connectivity information from a single mass-selected precursor ion population. *Analyst* **2017,** *142* (24), 4691-4702.

45. Wei, J.; Wu, J.; Tang, Y.; Ridgeway, M. E.; Park, M. A.; Costello, C. E.; Zaia, J.; Lin, C., Characterization and Quantification of Highly Sulfated Glycosaminoglycan Isomers by Gated-Trapped Ion Mobility Spectrometry Negative Electron Transfer Dissociation MS/MS. *Anal. Chem.* **2019,** *91* (4), 2994-3001.

46. Theisen, A.; Black, R.; Corinti, D.; Brown, J. M.; Bellina, B.; Barran, P. E., Initial Protein Unfolding Events in Ubiquitin, Cytochrome c and Myoglobin Are Revealed with the Use of 213 nm UVPD Coupled to IM-MS. *J. Am. Soc. Mass Spectrom.* **2019,** *30* (1), 24-33.

47. Stiving, A. Q.; Harvey, S. R.; Jones, B. J.; Bellina, B.; Brown, J. M.; Barran, P. E.; Wysocki, V. H., Coupling 193 nm Ultraviolet Photodissociation and Ion Mobility for Sequence Characterization of Conformationally-Selected Peptides. *J. Am. Soc. Mass Spectrom.* **2020,** *31* (11), 2313-2320.

48. Zucker, S. M.; Lee, S.; Webber, N.; Valentine, S. J.; Reilly, J. P.; Clemmer, D. E., An ion mobility/ion trap/photodissociation instrument for characterization of ion structure. *J. Am. Soc. Mass Spectrom.* **2011,** *22* (9), 1477-1485.

49. Warnke, S.; Baldauf, C.; Bowers, M. T.; Pagel, K.; von Helden, G., Photodissociation of conformer-selected ubiquitin ions reveals site-specific cis/trans isomerization of proline peptide bonds. *J. Am. Chem. Soc.* **2014,** *136* (29), 10308-10314.

50. Le, T.; Jeanne Dit Fouque, K.; Santos-Fernandez, M.; Navo, C. D.; Jimenez-Oses, G.; Sarksian, R.; Fernandez-Lima, F. A.; van der Donk, W. A., Substrate Sequence Controls Regioselectivity of Lanthionine Formation by ProcM. *J. Am. Chem. Soc.* **2021,** *143* (44), 18733-18743.

51. Pu, Y.; Ridgeway, M. E.; Glaskin, R. S.; Park, M. A.; Costello, C. E.; Lin, C., Separation and Identification of Isomeric Glycans by Selected Accumulation-Trapped Ion Mobility Spectrometry-Electron Activated Dissociation Tandem Mass Spectrometry. *Anal. Chem.* **2016,** *88* (7), 3440-3443.

52. Morrison, K. A.; Clowers, B. H., Differential Fragmentation of Mobility-Selected Glycans via Ultraviolet Photodissociation and Ion Mobility-Mass Spectrometry. *J. Am. Soc. Mass Spectrom.* **2017,** *28* (6), 1236-1241.

53. Voinov, V. G.; Deinzer, M. L.; Barofsky, D. F., Electron capture dissociation in a linear radiofrequency-free magnetic cell. *Rapid Commun. Mass Spectrom.* **2008,** *22* (19), 3087-3088.

54. Gadkari, V. V.; Ramirez, C. R.; Vallejo, D. D.; Kurulugama, R. T.; Fjeldsted, J. C.; Ruotolo, B. T., Enhanced

Collision Induced Unfolding and Electron Capture Dissociation of Native-like Protein Ions. *Anal. Chem.* **2020,** *92* (23), 15489-15496.

55. Jeanne Dit Fouque, K.; Wellmann, M.; Leyva Bombuse, D.; Santos-Fernandez, M.; Cintron-Diaz, Y. L.; Gomez-Hernandez, M. E.; Kaplan, D.; Voinov, V. G.; Fernandez-Lima, F., Effective discrimination of gas-phase peptide conformers using TIMS-ECD-ToF MS/MS. *Anal. Methods* **2021,** *13* (43), 5216-5223.

56. Simon, A. L.; Chirot, F.; Choi, C. M.; Clavier, C.; Barbaire, M.; Maurelli, J.; Dagany, X.; MacAleese, L.; Dugourd, P., Tandem ion mobility spectrometry coupled to laser excitation. *Rev. Sci. Instrum.* **2015,** *86* (9), 094101.

57. Liu, F. C.; Ridgeway, M. E.; Winfred, J.; Polfer, N. C.; Lee, J.; Theisen, A.; Wootton, C. A.; Park, M. A.; Bleiholder, C., Tandem-trapped ion mobility spectrometry/mass spectrometry coupled with ultraviolet photodissociation. *Rapid Commun Mass Spectrom.* **2021,** *35* (22), e9192.

58. Ross, A. C.; Vederas, J. C., Fundamental functionality: recent developments in understanding the structure-activity relationships of lantibiotic peptides. *J. Antibiot.* **2011,** *64* (1), 27-34.

59. Zhang, Q.; Yu, Y.; Velasquez, J. E.; van der Donk, W. A., Evolution of lanthipeptide synthetases. *Proc. Natl. Acad. Sci. USA* **2012,** *109* (45), 18361-18366.

60. Knerr, P. J.; van der Donk, W. A., Chemical synthesis and biological activity of analogues of the lantibiotic epilancin 15X. *J. Am. Chem. Soc.* **2012,** *134* (18), 7648-7651.

61. Jenuwein, T.; Allis, C. D., Translating the histone code. *Science* **2001,** *293* (5532), 1074-1080.

62. Bannister, A. J.; Kouzarides, T., Regulation of chromatin by histone modifications. *Cell Res.* **2011,** *21* (3), 381-95.

63. Williamson, E. A.; Wray, J. W.; Bansal, P.; Hromas, R., Overview for the histone codes for DNA repair. *Prog. Mol. Biol. Transl. Sci.* **2012,** *110*, 207-227.

64. Theisen, A.; Yan, B.; Brown, J. M.; Morris, M.; Bellina, B.; Barran, P. E., Use of Ultraviolet Photodissociation Coupled with Ion Mobility Mass Spectrometry To Determine Structure and Sequence from Drift Time Selected Peptides and Proteins. *Anal. Chem.* **2016,** *88* (20), 9964-9971.

65. Hernandez, D. R.; Debord, J. D.; Ridgeway, M. E.; Kaplan, D. A.; Park, M. A.; Fernandez-Lima, F., Ion dynamics in a trapped ion mobility spectrometer. *Analyst* **2014,** *139* (8), 1913-1921.

66. Ridgeway, M. E.; Lubeck, M.; Jordens, J.; Mann, M.; Park, M. A., Trapped ion mobility spectrometry: A short review. *Int. J. Mass Spectrom.* **2018,** *425*, 22-35.

67. Michelmann, K.; Silveira, J. A.; Ridgeway, M. E.; Park, M. A., Fundamentals of trapped ion mobility spectrometry. *J. Am. Soc. Mass Spectrom.* **2015,** *26* (1), 14-24.

68. Benigni, P.; Porter, J.; Ridgeway, M. E.; Park, M. A.; Fernandez-Lima, F., Increasing Analytical Separation and Duty Cycle with Nonlinear Analytical Mobility Scan Functions in TIMS-FT-ICR MS. *Anal. Chem.* **2018,** *90* (4), 2446-2450.

69. Repka, L. M.; Chekan, J. R.; Nair, S. K.; van der Donk, W. A., Mechanistic Understanding of Lanthipeptide Biosynthetic Enzymes. *Chem. Rev.* **2017,** *117* (8), 5457-5520.

70. Tang, W.; van der Donk, W. A., Structural characterization of four prochlorosins: a novel class of lantipeptides produced by planktonic marine cyanobacteria. *Biochemistry* **2012,** *51* (21), 4271-4279.

71. Bobeica, S. C.; Zhu, L.; Acedo, J. Z.; Tang, W.; van der Donk, W. A., Structural determinants of macrocyclization in substrate-controlled lanthipeptide biosynthetic pathways. *Chem. Sci.* **2020,** *11*, 12854-12870.

72. Yu, Y.; Mukherjee, S.; van der Donk, W. A., Product Formation by the Promiscuous Lanthipeptide Synthetase ProcM is under Kinetic Control. *J. Am. Chem. Soc.* **2015,** *137* (15), 5140-5148.

73. Cannon, J. R.; Martinez-Fonts, K.; Robotham, S. A.; Matouschek, A.; Brodbelt, J. S., Top-down 193-nm ultraviolet photodissociation mass spectrometry for simultaneous determination of polyubiquitin chain length and topology. *Anal. Chem.* **2015,** *87* (3), 1812-1820.

74. Morrison, L. J.; Rosenberg, J. A.; Singleton, J. P.; Brodbelt, J. S., Statistical Examination of the a and a + 1 Fragment Ions from 193 nm Ultraviolet Photodissociation Reveals Local Hydrogen Bonding Interactions. *J. Am. Soc. Mass Spectrom.* **2016,** *27* (9), 1443-1453.

75. Sidoli, S.; Garcia, B. A., Middle-down proteomics: a still unexploited resource for chromatin biology. *Expert Rev. Proteomics* **2017,** *14* (7), 617-626.

76. Tvardovskiy, A.; Schwammle, V.; Kempf, S. J.; Rogowska-Wrzesinska, A.; Jensen, O. N., Accumulation of histone variant H3.3 with age is associated with profound changes in the histone methylation landscape. *Nucleic Acids Res.* **2017,** *45* (16), 9272-9289.

77. Seligson, D. B.; Horvath, S.; Shi, T.; Yu, H.; Tze, S.; Grunstein, M.; Kurdistani, S. K., Global histone modification patterns predict risk of prostate cancer recurrence. *Nature* **2005,** *435* (7046), 1262-1266.

78. Yörüker, E. E.; Holdenrieder, S.; Gezer, U., Potential of circulating nucleosome-associated histone modifications in cancer. *Transl. Cancer Res.* **2018,** *7* (S2), S185-S191.

79. Garabedian, A.; Baird, M. A.; Porter, J.; Jeanne Dit Fouque, K.; Shliaha, P. V.; Jensen, O. N.; Williams, T. D.; Fernandez-Lima, F.; Shvartsburg, A. A., Linear and Differential Ion Mobility Separations of Middle-Down Proteoforms. *Anal. Chem.* **2018,** *90* (4), 2918-2925.

For Table of Contents Only